Journal of Power Sources 196 (2011) 9154–9163

Contents lists available at ScienceDirect

Journal of Power Sources

journal homepage: www.elsevier.com/locate/jpowsour

Effect of sintering aids on the conductivity of $BaCe_{0.9}Ln_{0.1}O_{3-\delta}$

M. Amsif[a], D. Marrero-López[b,*], J.C. Ruiz-Morales[a], S.N. Savvin[a], P. Núñez[a,*]

[a] Dpto. de Química Inorgánica, Universidad de la Laguna, 38200 Tenerife, Spain
[b] Dpto. de Física Aplicada I, Laboratorio de Materiales y Superficies (Unidad Asociada al C.S.I.C.), Universidad de Málaga, 29071 Málaga, Spain

ARTICLE INFO

Article history:
Received 1 February 2011
Received in revised form 4 April 2011
Accepted 22 June 2011
Available online 6 August 2011

Keywords:
$BaCeO_3$
SOFC
Conductivity
Electrolyte
Sintering aids

ABSTRACT

Polycrystalline powders of $BaCe_{0.9}Ln_{0.1}O_{3-\delta}$ (Ln = La, Nd, Sm, Gd, Yb, Tb and Y) have been prepared using a freeze-drying precursor route at 1000 °C. In order to decrease the densification temperature, different sintering aids (e.g. Co, Zn, Ni, Fe and Cu) were added by mixing the polycrystalline powders with a nitrate solution containing these metals. This allows obtaining dense ceramics at temperatures as low as 1000 °C, when compared to samples without sintering aids at 1400 °C. The effect of aid content and sintering temperature on the microstructure and electrical conductivity were investigated by scanning electron microscopy and impedance spectroscopy. The addition of small amounts of transition metals does not produce observable structural changes by conventional X-ray powder diffraction. However, the bulk and total conductivities decrease when compared to samples without transition metals. Zn seems to be the most effective sintering element for $BaCe_{0.9}Ln_{0.1}O_{3-\delta}$ electrolytes because it does not cause significant changes in the ionic and electronic conductivities.

1. Introduction

Proton conductors based on $BaCeO_3$ are promising candidates for intermediate temperature fuel cells (IT-SOFC) due to the fact that they exhibit higher ionic conductivity than oxide ion conductors, such as those based on ZrO_2 and CeO_2, below 600 °C [1–5].

Partial substitution of Ce^{4+} by rare-earth elements in $BaCeO_3$ (e.g. Y^{3+}, Gd^{3+}, Sm^{3+}, La^{3+}, etc.) introduces oxygen vacancies into the perovskite structure and enhances the ionic conductivity. The highest conductivity values have been found for Y^{3+} and Gd^{3+} doping, which produces smaller lattice distortion and larger free volume for ion mobility [6–11]. In these materials, the proton conductivity is dominant at low temperature, whereas oxide ion conductivity is the main contribution at high temperature [12,13]. In addition, n-type and p-type electronic conductivities are also observed at high temperature, limiting the application of cerates as solid electrolytes above 700 °C.

Solid electrolytes for SOFCs must have low porosity at the lowest sintering temperature as possible. Low temperature processing has additional advantages concerning the thermomechanical and electrical performance of the ceramics. In addition, co-firing $BaCeO_3$-based electrolytes with other SOFCs components would allow reducing fabrication processes and costs.

The synthesis of doped-$BaCeO_3$ is usually carried out by the conventional ceramic route, which requires high sintering temperature as 1600 °C to obtain high densification. This method has additional disadvantages, such as formation of undesirable phases, poor chemical homogeneity and large grain ceramic sizes, affecting negatively to the electrical and mechanical properties. In addition, evaporation of BaO has also been detected when the sintering temperature exceeds 1500 °C, thus reducing the sintering temperature is particularly important for these materials [14]. A wide range of synthesis methods have been proposed in order to decrease the synthesis temperature of doped $BaCeO_3$, such as citric acid [15,16], Pechini [17], oxalate [18] and freeze-drying [19], nevertheless, the sintering temperature to prepare dense ceramic materials is still relatively high, about 1400 °C.

It is well known that the introduction of sintering aids is an useful method in order to decrease the sintering temperature of the ceramic materials. This method has been widely used for the preparation of ceria based electrolytes [20,21], barium cerates [22–24] and barium zirconates [25–27]. In this sense, small amounts of some transition metals (e.g. Cu, Ni, Fe, Ti, Co, etc.) improve the sinterability of doped barium cerates [22–24,28–30]. For instance, Gorbova et al. [28] have prepared dense $BaCe_{0.9}Gd_{0.1}O_{3-\delta}$ ceramics without additives at 1600 °C and this temperature was reduced to 1450 °C after the addition of 1 mol% of transition metals. Furthermore, Costa et al. [30] obtained dense ceramics of $BaCe_{0.9}Y_{0.1}O_{3-\delta}$ with 4 mol% of NiO at 1250 °C. In general, these sintering additives improve the densification, but their effects on the total conductivity are debatable due to the different relative density between samples with and without sintering aids [24,28]. On the other hand,

* Corresponding authors. Tel.: +34 922318501; fax: +34 922318461.
E-mail addresses: damarre@uma.es (D. Marrero-López), pnunez@ull.es (P. Núñez).

0378-7753/$ – see front matter © 2011 Elsevier B.V. All rights reserved.
doi:10.1016/j.jpowsour.2011.06.086

the exact role of these sintering aids on the bulk and grain boundary conductivities is still not well known.

The effect of the incorporation of minor amounts of transition metals in barium cerate structure is a very important issue. For instance, NiO is usually used as component in the anode material of a SOFC. The NiO–electrolyte composite requires a sintering temperature of 1400 °C in order to get a good adherence to the electrolyte; and during this process a significant amount of Ni might diffuse inside the electrolyte. Therefore, it is essential to study the possible changes in the structure and transport properties of $BaCeO_3$ based electrolytes after the incorporation of minor transition metal (e.g. Ni, Fe, Co, etc.) into the perovskite structure of $BaCeO_3$, because most of the electrode materials used in SOFCs contain these elements. Moreover, the introduction of transition metals with variable oxidation states might produce significant changes in the ionic and electronic conductivity that should be examined.

In this work, $BaCe_{0.9}Ln_{0.1}O_{3-\delta}$ powders were prepared by a freeze-drying precursor method at a relatively low temperature of 1000 °C. Different sintering aids (Zn, Co, Cu, Ni and Fe) in the form of nitrate solutions were added to lower the densification temperature. The influence of these sintering additives on the microstructure, grain interior and grain boundary conductivities of $BaCe_{0.9}Ln_{0.1}O_{3-\delta}$ series are studied by impedance spectroscopy. Among the different sintering aids investigated, Zn resulted to be the most effective element for enhancing barium cerate densification and it was further investigated.

2. Experimental

2.1. Synthesis

Polycrystalline powders of $BaCe_{0.9}Ln_{0.1}O_{3-\delta}$ (Ln = La, Nd, Sm, Gd, Y, Yb and Tb) were prepared by a freeze-dried precursor route. The reactants were high purity metal nitrates supplied for Aldrich: $Ba(NO_3)_2$ (+99%), $Ce(NO_3)_3{\cdot}6H_2O$ (99.99%) and $Ln(NO_3)_3{\cdot}6H_2O$ (99.99%). They were previously studied by thermogravimetric analysis (Perkin Elmer, mod. Pyris Diamond) to determine the correct cation composition. Stoichiometric quantities of these reactants were dissolved in distilled water and then ethylenediaminetetraacetic acid (EDTA) (99.7% Aldrich) was added as complex agent to prevent precipitation in a 1:1 molar ratio ligand:metal. The pH was adjusted at 7 by adding ammonia and the cation concentration in the solutions was 0.15 M of Ba^{2+}. The solutions were frozen dropwise in liquid nitrogen and then dried in a HetoLyolab freeze-dryer for 3 days. The obtained amorphous precursors are very hygroscopic, so that they were immediately fired at 300 °C to prevent rehydration and to produce the combustion of the organic matter. Finally, the powders were calcined in alumina crucibles at 1000 °C to achieve crystallization. Under these synthesis conditions all the compounds were single phases [11]. The as-prepared oxide powders at 1000 °C, without sintering aids, were pressed at 125 MPa into disks of 10 mm diameter and 1.5 mm thickness and sintered at 1400 °C for 4 h in air. The relative density of these pellets was higher than 95%.

Samples with sintering aids were prepared using the polycrystalline powders fired at 1000 °C. They were mixed with the sintering aids in quantities between 0.5 and 5 mol%, in the form of an ethanolic solution of metal nitrates (Co, Cu, Ni, Zn and Fe), dried in air and then calcined at 550 °C for 1 h to decompose the nitrates to metal oxides. After that, the powders were used to prepare ceramic pellets, which were sintered between 950 and 1300 °C for 10 h. The relative density was calculated from the mass, volume of the pellets and the theoretical density obtained from the structural parameters by Rietveld analysis.

2.2. Structural and microstructural characterisation

Room temperature X-ray diffraction (XRD) patterns were collected with a PANalytical X'Pert Pro diffractometer, with CuKα radiation and the X'Celerator detector. Structure refinements and phase identification were performed using the X'PertHighScore Plus software [31].

The morphology of the sintered pellets was observed using a Scanning Electron Microscope (Jeol Ltd., JSM-6300). All samples were covered with a sputtered thin film of gold to avoid charging problems and to obtain better image definition. The average grain size of sintered pellets was estimated from the SEM micrographs, using the linear intercept method with the help of an image-analysis software [32].

2.3. Electrical characterisation

The electrical characterisation of the pellets was performed by impedance spectroscopy under humidified gases of air and 5% H_2–Ar mixture. The gases were humidified using a gas-washer at a temperature of 20 °C to ensure constant water content of about 2%.

The ceramic pellets were painted with Pt-ink (Metalor) as current collector on each side of the pellet and then fired at 800 °C for 30 min. The impedance diagrams were acquired on a 1260 Solartron Impedance Analyser between 100 and 750 °C in the 0.1–10^6 Hz frequency range.

The impedance diagrams were fitted with equivalent circuits using the program ZView [33] to study separately the bulk and grain-boundary contributions to the conductivity.

Conductivity dependence as a function of oxygen partial pressure (pO_2) from 0.21 to $\sim 10^{-20}$ atm was obtained with an electrochemical cell, consisting of a YSZ tube closed at one end with platinum oxygen sensor and pump. The oxygen partial pressure was controlled using an electrochemical pump with a dc source (Yokogawa 7651). The oxygen partial pressure inside the cell was continuously monitored by an oxygen sensor placed close to the sample using a Keithley 2700 multimeter. Before starting measurements, the pellets were kept at 800 °C for 5 h while the system was flushed with humidified 5% H_2–Ar gas mixture. The samples were equilibrated at each oxygen partial pressure for at least 4 h before acquiring the impedance diagrams.

3. Results and discussion

3.1. Structure

The XRD patterns of $BaCe_{0.9}Gd_{0.1}O_{3-\delta}$ (BCG) ceramics with 2 mol% of transition metals and sintered at 1200 °C for 10 h are shown in Fig. 1. All materials show the orthorhombic perovskite-type structure and no additional diffraction peaks assignable to single metal oxides were detected. Thus, the transition metals are highly dispersed around the grain boundary or incorporated into the perovskite structure.

These phases were analyzed by the Rietveld method (Fig. 2) in the orthorhombic *Pmcn* space group (ICSD 72768). No appreciable structural changes were detected in any of the samples, even for compositions containing 5 mol% of Zn (Fig. 2a).

The lattice cell parameters for $BaCe_{0.9}Gd_{0.1}O_{3-\delta}$ compounds with sintering aids are summarised in Table 1. The cell volume of the different compounds changes only slightly with respect to samples without transition metals. Considering the bigger ionic radii of six coordinated Ce^{4+} than the one corresponding to the transition metals in the same coordination configuration, one would expect a decrease of the lattice cell if these elements are incorporated in the B-site of the perovskite structure. However, one can observe that

Table 1
Phase composition, sintering conditions, cell parameters, relative density and average grain size of $BaCe_{0.9}Gd_{0.1}O_{3-\delta}$ (BCG) ceramics without and with different sintering aids.

Compositions	Sintering conditions	Cell parameters				Relative density (%)	D_g (μm)
		a (Å)	*b* (Å)	*c* (Å)	*V* (Å^3)		
BCG	1400 °C/4 h	6.2239(2	8.7787(3)	6.2404(2)	340.95(2)	100	1.2
BCG–0.5% Zn	1200 °C/10 h	6.2241(3)	8.7794(4)	6.2426(3)	341.11(9)	93	0.5
BCG–2% Zn	1200 °C/10 h	6.2233(3)	8.7789(3)	6.2427(2)	341.06(2)	99	1.2
BCG–2% Zn_1000	1000 °C/10 h	6.2236(1)	8.7775(1)	6.2439(1)	341.09(3)	95	–
BCG–5% Zn	1200 °C/10 h	6.2248(3)	8.7835(4)	6.2441(3)	341.40(3)	97	1.5
BCG–2% Zn_1300	1300 °C/10 h	6.2230(1)	8.7793(2)	6.2400(1)	340.91(5)	100	–
BCG–2% Ni	1200 °C/10 h	6.2216(2)	8.7808(3)	6.2424(2)	341.02(3)	90	0.5
BCG–2% Cu	1200 °C/10 h	6.2228(3)	8.7802(4)	6.2419(3)	341.04(4)	98	1.1
BCG–2% Co	1200 °C/10 h	6.2147(4)	8.7768(6)	6.2318(4)	339.92(1)	100	1.1

the cell volume for Zn-containing samples increases slightly with the increase of Zn from 341.11(9) Å^3 for 0.5 mol% to 341.40(3) Å^3 for 5 mol%, indicating that a fraction of Zn is incorporated in the perovskite structure rather than segregated at the grain boundary. This increase of the cell volume is contrary to the expected, taking into account the smaller ionic radii of Zn^{2+} (0.74 Å) compared to Ce^{4+} (0.87 Å) in the six coordinated state. It should be also considered that the formation of oxygen vacancies after Zn^{2+} incorporation into the perovskite structure may cause lattice expansion. Hence, the shrinkage of the structure with the incorporation of a smaller transition metal cation than Ce^{4+} and the expansion of the cell due to the formation of oxygen vacancies result in only a small variation of the cell volume. Furthermore, the cell volume for the different samples also increases with the sintering temperature due to an enhancement of metal transition solubility with the temperature.

Several works have reported that the solubility of the transition metals in $BaCeO_3$ electrolytes is rather low. Indeed, the NiO solubility for $BaCe_{0.9}Y_{0.1}O_{2.95}$ was estimated to be about 0.4 mol% and EDS analysis suggested enrichment of boundary layers with transition metal oxides [30].

The study of the bulk conductivity as a function of the metal content and sintering temperature, in the next sections, will provide further insights on the incorporation of these transition metals into the perovskite structure.

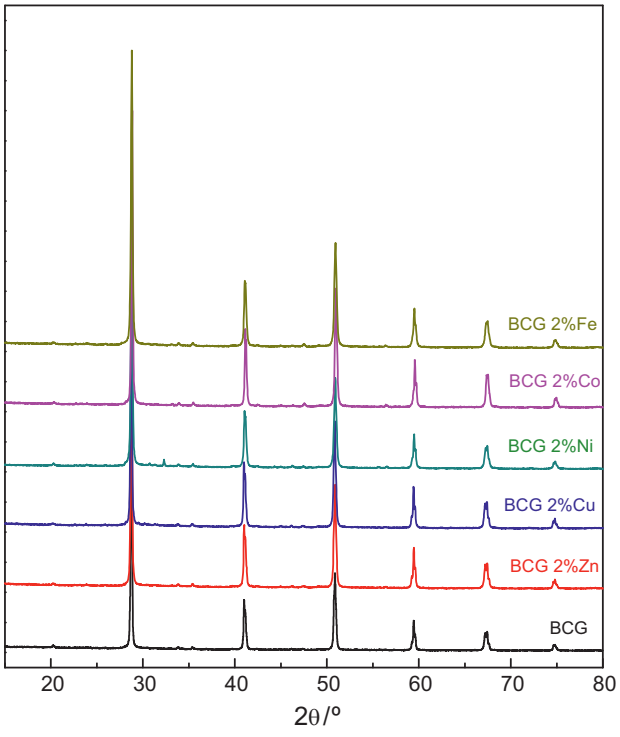

Fig. 1. XRD patterns of $BaCe_{0.9}Gd_{0.1}O_{3-\delta}$ with different sintering aids and sintered at 1200 °C.

3.2. Ceramic microstructure

Pellets without transition metals were sintered from the polycrystalline freeze-dried powders between 1200 and 1400 °C for 4 h. Samples sintered at 1300 °C have a relative density of 85% and increases up to 95% at 1400 °C.

The results shown in Table 1 confirm that small amounts of transition metals have a great effect on the sintering of $BaCeO_3$-based electrolytes, in agreement with previous works [28–30]. Samples sintered at 1200 °C for 10 h with 2 mol% of Zn, Cu and Co resulted in dense pellets with a relative density higher than 98%. In contrast, samples with Ni and Fe showed a lower relative density of 90 and 77%, respectively. This last sample was not further characterized due to its relatively low density. It should be commented

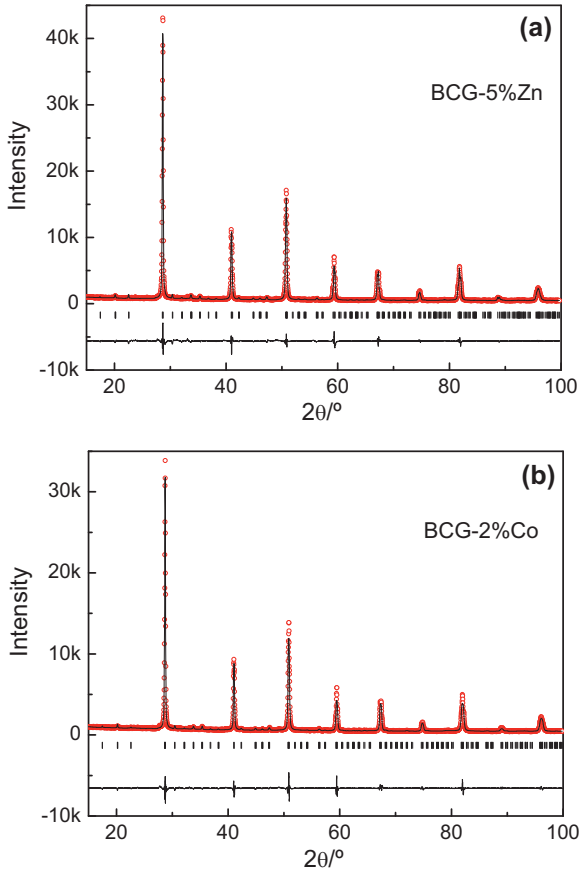

Fig. 2. Rietveld refinements for (a) BCG-5% Zn and (b) BCG-2% Co samples.

that a similar behavior was previously found in barium zirconates, where samples with Ni and Fe showed lower density than those containing Zn and Co [25].

SEM images of BCG samples without and with sintering aids are shown in Fig. 3. The SEM images show ceramic materials with low porosity. No detectable traces of impurities or phase segregations at the grain boundaries were found in any of the samples studied. In general, the addition of transition metals does not affect significantly the microstructure of the pellets, even the grain size is similar, despite the lower sintering temperature used in samples with transition metals. The average grain size, given in Table 1, does not depend significantly on the type of additive used with values around 1.1 μm for Zn, Cu and Co-containing samples compared to 1.2 μm for pure BCG. In contrast, Ni-containing sample with the lowest grade of densification exhibits the smallest grain size of about 0.5 μm (Table 1). Hence, samples without and with sintering aids exhibit similar grain size, indicating that sintering aids promote densification but also grain growth rate at low temperature.

In order to study the influence of the aid content and temperature on the densification of BCG materials, different quantities of Zn^{2+} between 0.5 and 5 mol% were used to prepare pellets in the temperature range between 950 and 1200 °C. At 1200 °C the relative density of samples with 0.5 mol% of Zn is around 92% and higher Zn-content increases the densification up to almost 100%. The SEM images confirm that the sample with 0.5 mol% of Zn shows visible porosity (Fig. 4a) at least on the surface, in contrast to samples with higher amounts of Zn (Fig. 4b–d). Furthermore, the grain size grows with Zn-content from 0.5 μm for 0.5 mol% to 1.5 μm for 5 mol% (Fig. 4).

On the other hand, the relative density of samples with 2 mol% of Zn is as high as 85% at 950 °C and it increases up to 95% at only 1000 °C. In the absence of second phases, detectable by XRD, sintering enhancement in these ceramic materials is believed to take place as a result of enhanced diffusion through the grain boundary, possibly because of cation vacancy formation in the intergranular regions [25].

This low sintering temperature of 1000–1200 °C is useful to prepare fuel cells based on barium cerates in only one step by co-sintering and it also prevents excessive reactivity with the electrode materials.

3.3. Electrical characterisation

3.3.1. Conductivity of BCG with 2 mol% of transition metals

Impedance diagrams for dense $BaCe_{0.9}Gd_{0.1}O_{3-\delta}$ (BCG) pellets sintered at 1200 °C with different transition metals in 2 mol% are shown in Fig. 5. Three different contributions are easily discernible in all the diagrams ascribed to grain interior (bulk), grain boundary and electrode processes. It is clear that the bulk and grain boundary contributions are strongly dependent on the sintering aid used. For all samples with transition metals both bulk and grain boundary resistances increase, especially for samples with Co (Fig. 5e), although minor changes are observed in samples with Zn (Fig. 5b).

The diagrams were fitted with an equivalent circuit consisting of two (RQ) elements and a pseudocapacitance in series to simulate the bulk, grain-boundary and electrode responses respectively. Thus, the following equivalent circuit was considered: $(R_1Q_1)(R_2Q_2)Q_3$. The grain boundary and grain interior processes were studied separately at temperatures lower than 250 °C. The electrode processes are dominant at higher temperatures and only the total conductivity was obtained from the interception of impedance diagrams with the Z'-axis at high frequency.

The capacitance C_i values were obtained from the resistance R_i and pseudocapacitance Q_i values using the following relation [34].

$$C_i = R_i^{1/n_i - 1} Q^{1/n_i} \quad (1)$$

The bulk, grain boundary and electrode contributions, normalized by the geometrical factor of the pellets L/S, show typical capacitance values of 1 pF cm^{-1}, 1 nF cm^{-1} and 10 μF cm^{-1} for the bulk, grain boundary and electrode processes respectively.

The grain interior R_b and grain boundary R_{gb} resistances were used to obtain the bulk and macroscopic grain boundary conductivity, taking into account the sample geometry $\sigma = L/(R{\cdot}S)$ and the corresponding values of conductivity were plotted using the Arrhenius equation:

$$\sigma = \frac{\sigma_0}{T} \cdot \exp\left(\frac{-E_a}{kT}\right) \quad (2)$$

The temperature dependence of grain interior conductivity in air is shown in Fig. 6a. As can be observed, the incorporation of different transition metals produces a decrease of the grain interior conductivity when compared to the sample without sintering aids. The lowest values of bulk conductivity, almost seven times smaller than pure BCG, were found for samples with Co addition (Table 2). This sample exhibits the lowest cell volume (Table 1), so that Co seems to produce a larger distortion of the perovskite structure reducing the ion mobility. Conversely, samples with Zn addition exhibit a cell volume comparable to pure BCG and therefore the largest bulk conductivity between the samples with transition metals (Table 2).

The activation energy for the bulk conductivity is almost constant for the different samples, ranging between 0.49 and 0.51 eV. (Table 2), being similar to that reported previously [22–24].

In the case of the grain boundary resistance, the largest values are found in Ni-containing samples with the lowest relative density and grain size (Fig. 6b). The other samples show also somewhat larger grain boundary resistance than pure BCG; and only BCG–2% Zn exhibits a grain boundary resistance close to that of pure BCG.

It should be considered that the grain boundary resistance depends on the grain size and consequently of number of boundaries across the sample. By considering a simple brick layer model [35–37] this becomes:

$$R_{gb} = \rho_{gb} \frac{\delta_{gb} N_{gb}}{A} \quad (3)$$

where ρ_{gb} is the grain boundary resistivity, δ_{gb} is the grain boundary thickness and $N_{gb} = L/d_g$ is the number of grain boundaries across the sample.

In this case, the different values of grain boundary resistance can not be only attributed to changes in the relative density and average grain size of the ceramics, because samples with and without sintering aids posses similar grain size between 0.5 and 1.5 μm and relative density higher than 90% (Table 1). This seems to indicate that the blocking effects at the grain boundary in samples with transition metals could be due to compositional differences rather than microstructural changes.

In order to evaluate the real effects of the sintering aids on the grain boundary resistance, the specific grain boundary conductivity was determined. This was obtained from the relaxation frequency $f_{gb} = (2\pi R_{gb} C_{gb})^{-1}$, assuming that the dielectric constant of the bulk and grain boundary contributions remains nearly unchanged, with a typical value of $\varepsilon_r = 37$ [38].

$$\sigma_{gb} = 2\pi f_{gb} \varepsilon_o \varepsilon_r$$

The temperature dependence of the specific grain boundary conductivity is represented in Fig. 6c. This graph shows a similar behavior to that observed in the macroscopic grain boundary resistance with the highest values of grain boundary conductivity for pure and Zn-containing samples (Table 2), while Ni-containing

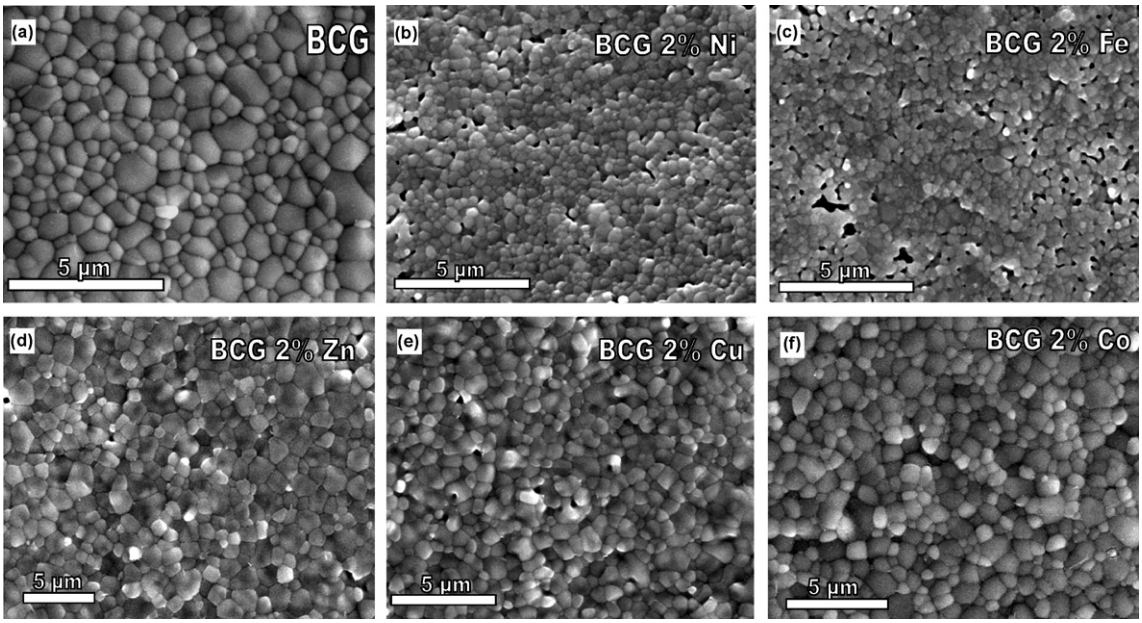

Fig. 3. SEM images of $BaCe_{0.9}Gd_{0.1}O_{3-\delta}$ pellets sintered at 1200 °C for 10 h with 2 mol% of different transition metals.

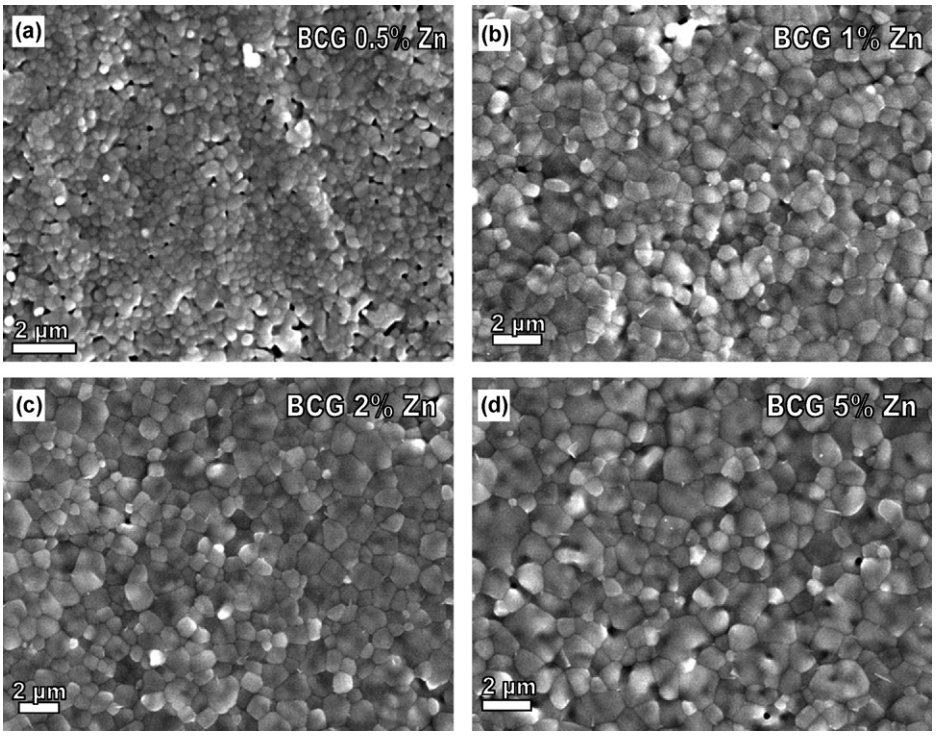

Fig. 4. SEM images of $BaCe_{0.9}Gd_{0.1}O_{3-\delta}$ pellets with different content of Zn and sintered at 1200 °C for 10 h.

Table 2
Conductivities and activation energies for the bulk, grain boundary and total contributions obtained from the impedance diagrams in air, using the sintering conditions as indicated in Table 1.

Composition	σ_{bulk} (mS cm^{-1})$^{200\,^{\circ}C/air}$	σ_{gb} (μS cm^{-1})$^{200\,^{\circ}C/air}$	σ_t (mS cm^{-1})$^{600\,^{\circ}C/air}$	E_{bulk} (eV)^{air}	E_{gb} (eV)^{air}	δ_{gb} (nm)^{air}
BCG	0.29	0.57	18.4	0.49	0.67	3.5
BCG–0.5% Zn	0.13	0.39	7.8	0.49	0.73	2.1
BCG–2% Zn	0.20	0.72	11.0	0.50	0.69	3.5
BCG–5% Zn	0.15	0.38	9.4	0.52	0.66	4.6
BCG–2% Zn_1300	0.16	–	10.2	0.52	0.76	–
BCG–2% Ni	0.17	0.09	7.2	0.50	0.67	2.8
BCG–2% Cu	0.18	0.33	10.3	0.51	0.68	3.3
BCG–2% Co	0.05	0.23	3.5	0.50	0.69	5.1

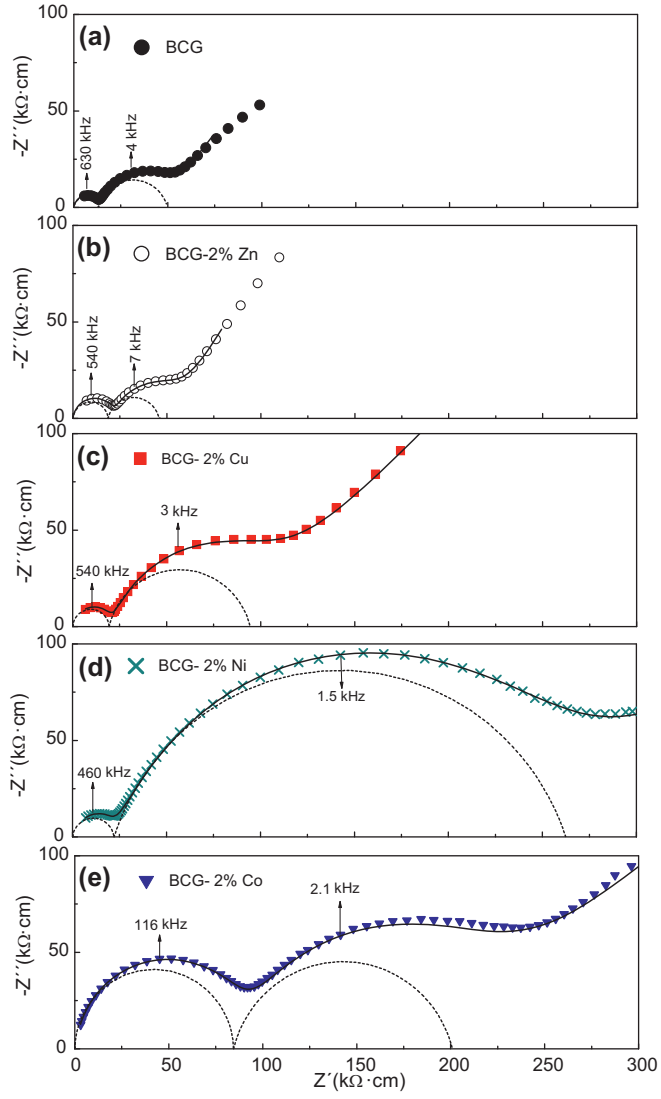

Fig. 5. Impedance diagrams acquired at 150 °C in wet air for $BaCe_{0.9}Gd_{0.1}O_{3-\delta}$ pellets sintered at 1200 °C for 10 h with different sintering aids. The solid line was obtained by fitting the data with equivalent circuits and dashed lines are the deconvolution of the bulk and grain boundary contributions.

samples exhibit the lowest values of specific grain boundary conductivity. The activation energy of the grain boundary conductivity is somewhat higher for those samples with sintering aids, increasing from 0.67 eV for pure BCG to 0.69 eV for BCG–2% Co.

The grain boundary width δ_{gb} has been also estimated using the following relation:

$$\delta_{gb} = \frac{\varepsilon_o \varepsilon_b}{C_{gb}} \frac{d_g S}{L} \quad (4)$$

This takes a value of 3.5 nm for pure BCG and varies between 2.8 nm for Ni to 5.1 nm for Co-containing samples with 2 mol%. On the other hand, δ_{gb} seems to increase with Zn addition and grain size from 2.1 nm for BCG–0.5% Zn to 4.6 nm for BCG–5% Zn sintered at 1200 °C (Table 2). Thus, the significant differences in the grain boundary resistance between samples with or without sintering aids cannot be only attributed to changes in grain size or grain boundary thickness, but compositional changes at the grain boundary as also occurs with the bulk conductivity.

The Arrhenius plots of the total conductivity, under humidified air and 5% H_2–Ar gas mixture, are shown in Fig. 7. In general, the sintering aids decrease the total conductivity, although Zn addition has the lowest effects on the total conductivity with a value of 11.0 mS cm^{-1} for BCG–2% Zn in humidified air at 600 °C compared to 18.4 mS cm^{-1} for pure BCG under the same conditions. It should be noted that the differences in conductivity are more significant in the high temperature range. This is due the fact that the bulk conduction is dominant at high temperature and decreases after the incorporation of transition metals in the perovskite structure. The other samples exhibit lower values of total conductivity than pure BCG and specially those containing Ni and Co additives. Conductivity data in humidified air at 600 °C are given in Table 2.

The conductivity in humidified 5% H_2–Ar gas enhances in the low temperature range due to an increase of the proton conductivity. This increase of conductivity is most significant for Ni and Co containing samples. A similar behavior was recently observed by Medvedev et al. [39], although it could be associated to an increase of the electronic conductivity due to the variable oxidation states of these elements and an increase of the electron hole concentration that may enhance the electronic contribution by electron polaron hopping. This will be studied in a next section.

It should be commented that the conductivity values obtained in this work for BCG with transition metals are somewhat lower than that previously reported (Table 3). This could be ascribed to the different preparation method, lower sintering temperature used here,

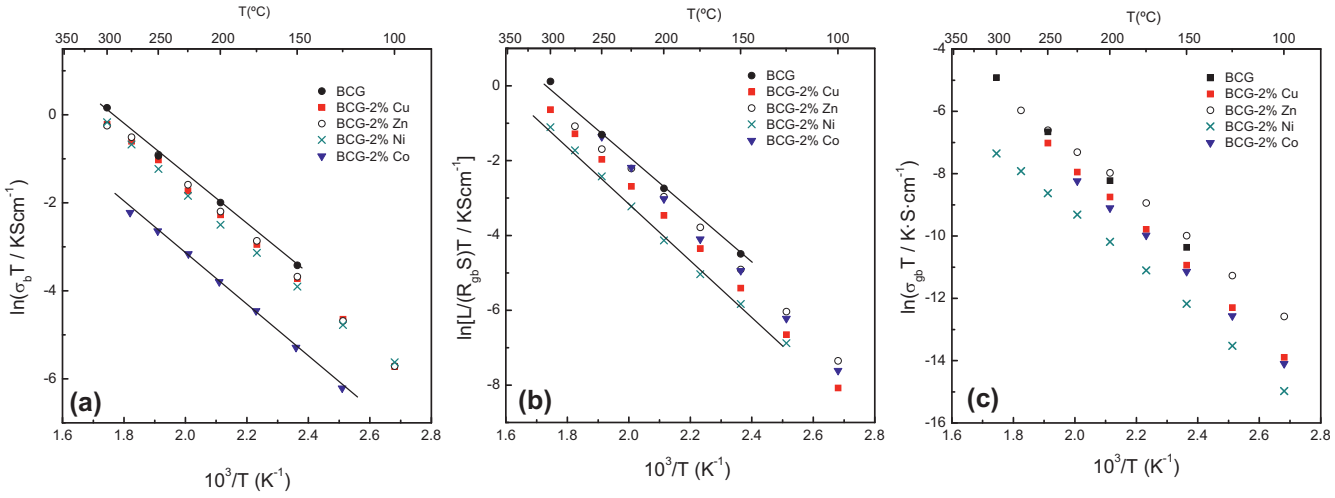

Fig. 6. Arrhenius plot of the (a) bulk, (b) grain boundary resistance and (c) grain boundary conductivities for BCG samples with and without sintering aids in humidified air atmosphere.

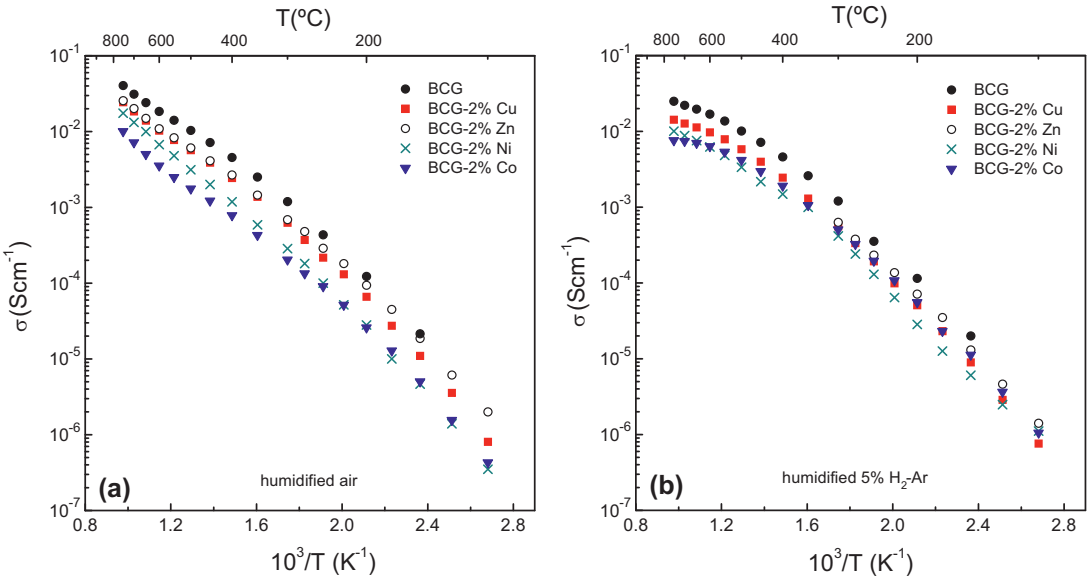

Fig. 7. Temperature dependence of the total conductivity for $BaCe_{0.9}Gd_{0.1}O_{3-\delta}$ samples sintered at 1200 °C with different aids in humidified (a) air and (b) 5% H_2–Ar.

different relative density of the samples and content of transition metals. It should be also considered that in previous works, the transition metals were introduced using oxide powders, which are less reactive than the nitrates used herein.

It is clear from the data of Table 3 that the lowest values of conductivity are found for BCG samples with Co, while the highest values are found for Zn and Cu-containing samples.

3.3.2. *Conductivity of $BaCe_{0.9}Ln_{0.1}O_{3-\delta}$ with Zn aids*

The samples with Zn-addition were further investigated as a function of the Zn-content and sintering temperature, because Zn causes minor spoiling changes in the conductivity of rare-earth doped $BaCeO_3$.

Fig. 8 shows the temperature dependence of the bulk and grain boundary conductivities of BCG samples sintered at 1200 °C as a function of Zn-content. As can be observed, the bulk conductivity decreases after Zn-addition, although there is not a clear dependence between the bulk conductivity and the Zn-content. One would expect lower values of bulk conductivity as the Zn-content increases, but contrary, the sample with only 0.5 mol% of Zn exhibits the lowest conductivity, which can be attributed to the lower relative density of this sample (Table 1).

The grain boundary resistance (Fig. 8b) is similar in all the cases, showing lower values for BCG–2% Zn due to the better grade of densification and the lower content of Zn necessary to obtain dense pellets at 1200 °C.

Total conductivity (Fig. 9) in both air and 5% H_2–Ar gases shows similar values for all the samples at low temperature, but differences are found in the high temperature range, exhibiting the sample without Zn addition higher values of conductivity (Table 2).

The bulk and total conductivities in $BaCe_{0.9}Ln_{0.1}O_{3-\delta}$ (Ln = La, Nd, Sm, Gd, Y and Yb) series show a maximum in conductivity for Gd-doped samples. The introduction of Zn produces a decrease of both bulk and total conductivities in all the samples (Fig. 10a and b).

The dependence of the conductivity as a function of the sintering temperature for a fixed amount of Zn-content was also investigated. For this purpose, samples with 2 mol% of Zn were sintered between 1000 and 1300 °C for 10 h, yielding dense samples with relative density higher than 98%. The bulk conductivity (Fig. 11a) seems to be independent on the sintering temperature used and lower than that of the pure sample. This indicates that a fraction of Zn is incorporated into the perovskite structure and the Zn solubility does not enhance significantly with the sintering temperature. This result is further supported by the nearly constant variation of the cell volume with temperature and Zn-content (Table 1).

The most important differences in the electrolyte resistance are found in the grain boundary contribution due to mainly the different average grain size with the sintering temperature. Samples sintered at lower temperatures have smaller grain size and consequently higher grain boundary resistance. Conversely, samples prepared with 2 mol% of Zn at 1300 °C show larger grain size and therefore lower grain boundary resistance.

As expected, the total conductivity (Fig. 12) increases with the sintering temperature and the differences in conductivity values are more important in the low temperature range due to the larger grain boundary resistance in samples prepared at low temperature

Table 3
Total conductivity values for BCG samples with different transition metals extracted from the literature.

Composition	σ_t (mS cm^{-1}) $^{600\,°C/air}$	Sintering temperature (°C)	Reference	σ_t (mS cm^{-1})$^{600\,°C/air}$ this work[a]
BCG	7.1	1600	[28]	18.4
BCG–2% Co	5.0	1450	[39]	3.54
BCG–1% Co	5.0	1450	[28]	–
BCY–4% Ni	10.0	1250	[30]	7.2
BCG–1% Ni	9.0	1450	[28]	–
BCG–1% Cu	16.0	1450	[28]	10.3
BCG–2% Cu	12.5	1450	[24]	10.3
BCG–1% Zn	10.5	1450	[28]	11.4

[a] Conductivity for BCG samples containing 2 mol% of transition metals and sintered at 1200 °C.

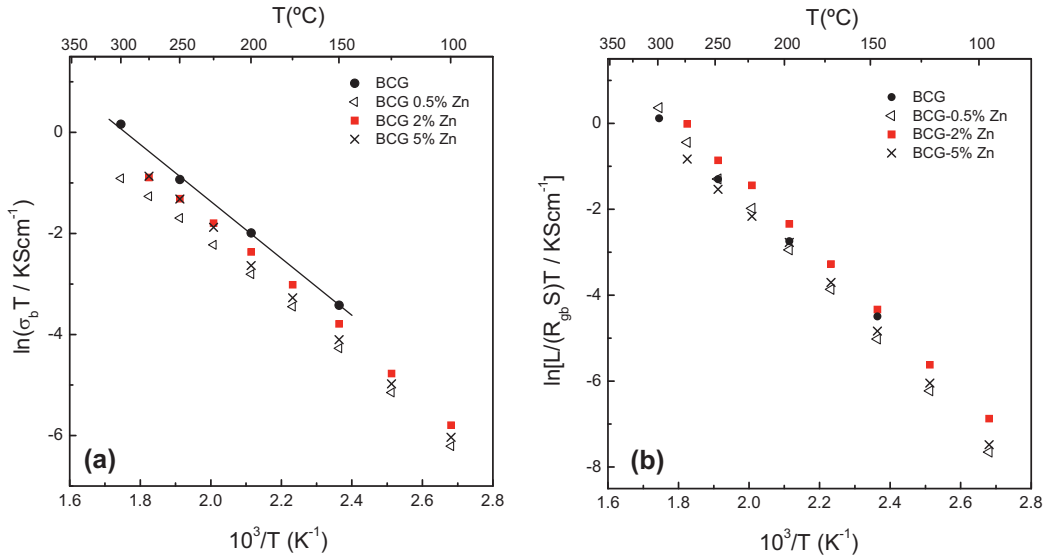

Fig. 8. Arrhenius plots of the (a) grain-interior conductivity and (b) grain-boundary resistance for $BaCe_{0.9}Gd_{0.1}O_{3-\delta}$ samples sintered at 1200 °C with different content of Zn.

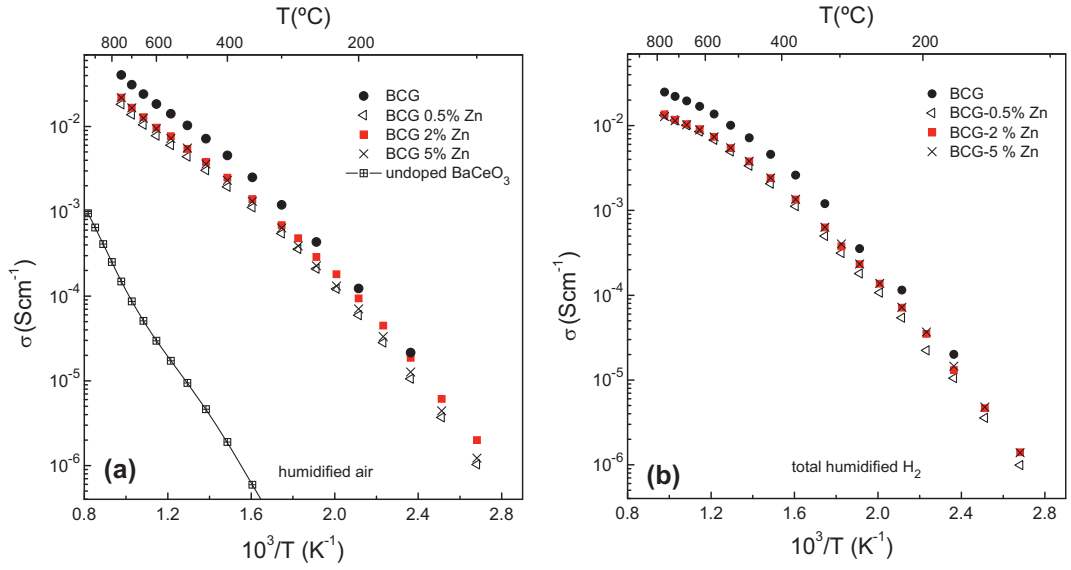

Fig. 9. Temperature dependence of the total conductivity for $BaCe_{0.9}Gd_{0.1}O_{3-\delta}$ samples sintered at 1200 °C with different content of Zn in humidified (a) air and (b) 5% H_2–Ar. The conductivity of undoped $BaCeO_3$ is also included for comparison.

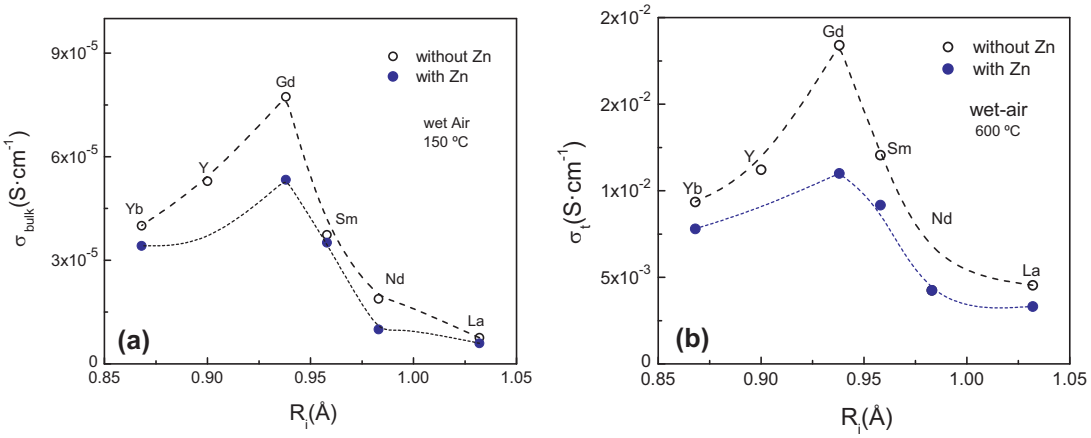

Fig. 10. Variation of the (a) bulk conductivity at 150 °C and (b) total conductivity at 600 °C for $BaCe_{0.9}Gd_{0.1}O_{3-\delta}$ samples without (open circles) and with 2 mol% of Zn (closed circles) as a function of the rare-earth ionic radius.

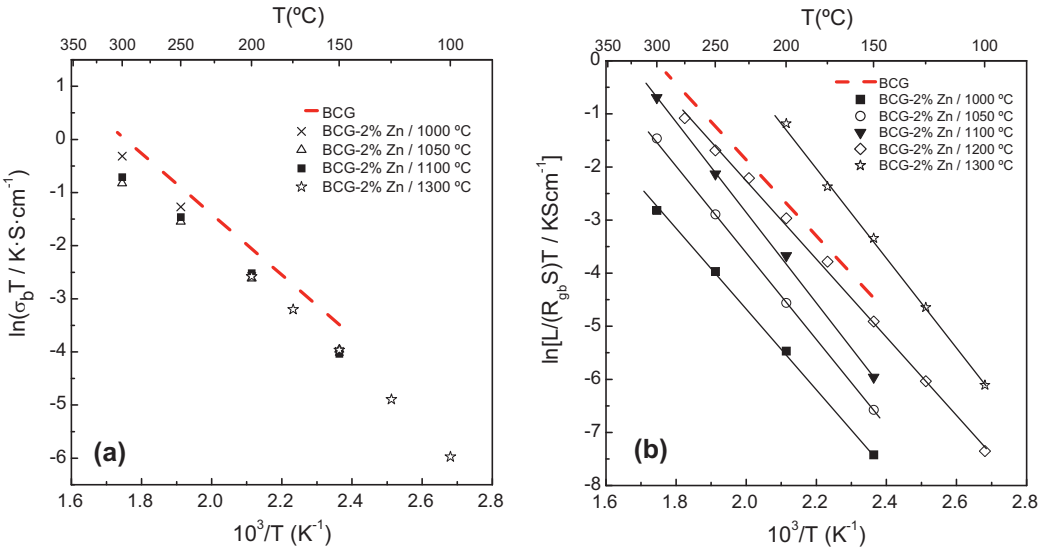

Fig. 11. Arrhenius plots of the (a) grain-interior conductivity and (b) grain-boundary resistance for $BaCe_{0.9}Gd_{0.1}O_{3-\delta}$ samples with 2 mol% of Zn and sintered between 1000 and 1300 °C.

with smaller grain size. In the high temperature range, the values of conductivity are less influenced by the grain boundary contribution and therefore they are comparable, although lower compared to samples without transition metals.

3.3.3. *Conductivity dependence with pO_2*

The conductivity as a function of the oxygen partial pressure for Gd-doped samples with and without sintering aids is shown in Fig. 13. The plateau region observed at low oxygen partial pressure pO_2 (<10^{-5} atm) is attributed to pure ionic conduction.

At the high pO_2 range of 10^{-5} – 0.21 atm the conductivity increases with pO_2, indicating that the conduction mechanism includes ionic and electronic p-type contributions. Holes are created in the perovskite structure by the incorporation of oxygen in the lattice, according to the equation:

$$\frac{1}{2}O_2 + V_O^{\bullet\bullet} = O_O^x + 2h^{\bullet} \quad (5)$$

Thus, the total conductivity can be approximated by the classical model, which includes ionic and p-type conductivities:

$$\sigma_t = \sigma_i + \sigma_p^o \cdot (pO_2)^{1/4} \quad (6)$$

where σ_i and σ_p^o are the values of ionic and partial p-type electronic conductivities at unit oxygen pressure. This model was used for fitting the σ vs pO_2 curves (Fig. 13).

It is obvious from Fig. 13 that samples containing transition metals show somewhat larger values of p-type conductivity when compared to pure BCG sample. This can be explained by the oxygen vacancies introduced in the lattice when Zn^{2+}, Ni^{2+} and especially $Cu^{1,2+}$ are incorporated in the Ce^{4+} position, creating more holes according to Eq. (5).

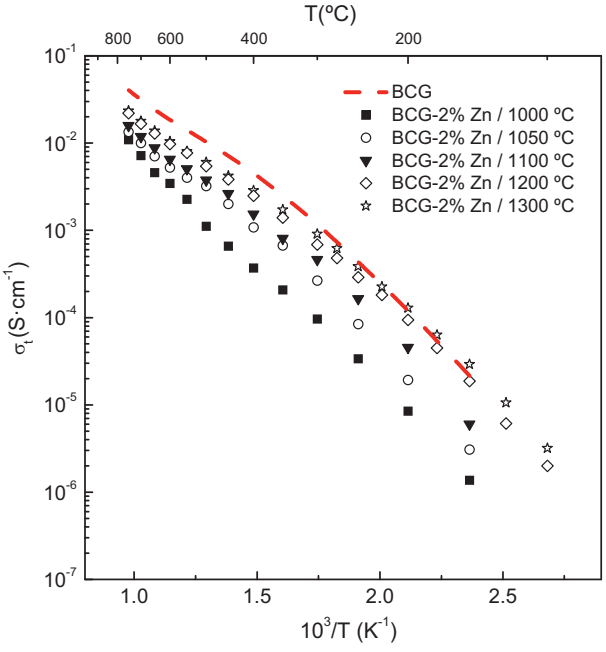

Fig. 12. Temperature dependence of the total conductivity for $BaCe_{0.9}Gd_{0.1}O_{3-\delta}$ samples with 2 mol% of Zn and sintered between 1000 and 1300 °C for 10 h.

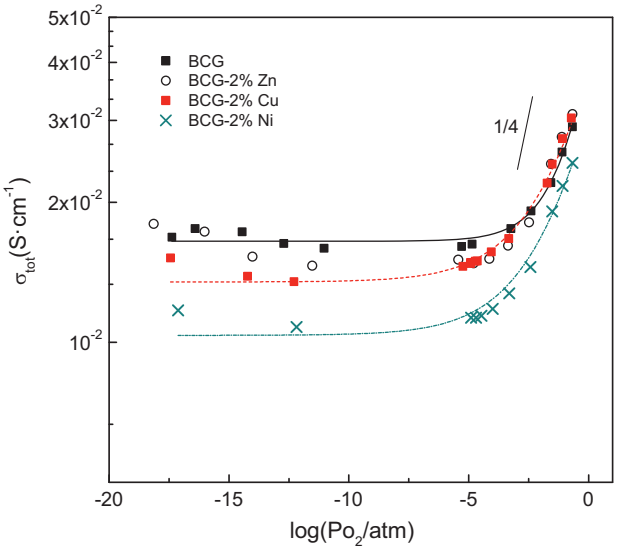

Fig. 13. Oxygen partial pressure dependence of the total conductivity at 800 °C for $BaCe_{0.9}Gd_{0.1}O_{3-\delta}$ samples containing different sintering aids. The solid lines are the fitting curve using (Eq. (6)).

It should be also noted that there is also a small increase of the total conductivity as the oxygen partial pressure decreases. This increase of conductivity at low pO_2 values is very small and does not follow the typical power law dependence with the oxygen partial pressure $(pO_2)^{-1/4}$. It is also remarkable that the conductivity for BCG without and with Zn (in Fig. 13) increases at lower pO_2 values, suggesting the presence of a minor proton contribution to the total conductivity at this temperature. Therefore, the non-plateau region at low oxygen partial pressure could be ascribed to both a change in the proton conductivity due to variation of the water partial pressure during the experiment; and also a slight increase of the n-type conductivity.

It should be also mentioned that the dependence of the total conductivity on pO_2 (Fig. 13) was obtained at relatively high temperature (800 °C). However, barium cerates have application as solid electrolytes below 700 °C, where the p-type conductivity is negligible, and the ionic conductivity is higher compared to that of ceria based electrolytes. Therefore, the electronic conductivity in samples with sintering aids is possible negligible in the low temperature range, increasing notably the electrolytic domain at low temperature, as also observed in ceria based electrolytes with cobalt as sintering aids [40]. However, the ionic transport numbers should be determined in the low temperature range to confirm this issue.

In addition, the dependence of the conductivity on pO_2 was only investigated for samples with high level content of transition metals (2 mol%) to study a possible enhancement of the electronic contribution at high temperature. Nevertheless, the content of transition metals in BCG samples could be reduced to only 0.5–1 mol% to obtain dense samples at 1000–1200 °C and consequently the electronic conductivity should be lower.

Zn-containing samples show only a slight increase in the p-type conductivity with respect to Ni and Cu containing samples and this is probably related to a minor incorporation of Zn^{2+} in the lattice, producing minor changes in the structure and consequently in the bulk, total and electronic conductivities.

These results seem to indicate that Zn is the best sintering aid to improve densification of $BaCeO_3$-based electrolytes without affecting considerably the ionic and electronic conductivities. This behavior is similar to that found previously in barium zirconates [25].

4. Conclusions

The effect of small additions of transition metals in $BaCe_{0.9}Ln_{0.1}O_{3-\delta}$ (Ln = La, Nd, Sm, Gd, Yb, Tb and Y) electrolytes on the microstructure and the transport properties was investigated. A homogeneous distribution of transition metals (e.g. Co, Fe, Ni, Zn and Cu) in the form of ethanolic solution of nitrates (0.5–5 mol%) was added to the polycrystalline powders of BCG obtained using the freeze-drying method, resulting in a significant reduction of the sintering temperature (1000–1200 °C) when compared to freeze-dried samples without transition metals (1400 °C). The addition of these transition metals improves both the densification and grain growth, yielding dense ceramic materials at 1000 °C for samples with Co, Cu and Zn addition. The cell volume, determined by XRD analysis, changes slightly after sintering the specimens between 1000 and 1200 °C, indicating that a fraction of transition metals are incorporated in the perovskite structure. Despite, the apparent low incorporation of these metals in the grain interiors, the bulk conductivity of BCG, modified with transition metals, is lower than samples without transition metals and especially for samples with cobalt. At the same time, the specific grain boundary conductivity decreases slightly. Although dense samples with transition metals are obtained at only 1000 °C, the total conductivity is reduced significantly compared to samples prepared at 1200 °C due to the higher grain boundary contribution as consequence of the smaller grain size. On the other hand, the non-desirable p-type conductivity also increases due to an increase of the oxygen vacancy concentration. Among the different transition metals studied, Zn produces minor changes in the total and electronic conductivities of barium cerates. These results indicate that dense barium cerates electrolytes could be obtained for fuel cells applications at relatively low temperature by optimizing the sintering temperature and Zn amounts.

Acknowledgements

This work was supported by the Spanish (MAT2007-60127 and MAT2010-16007) and Canary Islands (PI2007/020) Research programs.

References

[1] H. Iwahara, H. Uchida, K. Ono, K.J. Ogaki, J. Electrochem. Soc. 135 (1988) 529.
[2] H. Iwahara, Solid State Ionics 86–88 (1996) 9.
[3] N. Bonanos, K.S. Knight, B. Ellis, Solid State Ionics 79 (1995) 161.
[4] T. Norby, Solid State Ionics 125 (1999) 1.
[5] K.D. Kreuer, Annu. Rev. Res. 33 (2003) 333.
[6] H. Iwahara, T. Yajima, H. Ushida, Solid State Ionics 70–71 (1994) 267.
[7] D. Shima, S.M. Haile, Solid State Ionics 97 (1997) 443.
[8] F.L. Chen, O. Toft Sørensen, G.Y. Meng, D.K. Peng, J. Eur. Ceram. Soc. 18 (1998) 1389.
[9] N. Bonanos, B. Ellis, K.S. Knight, M.N. Mahmood, Solid State Ionics 35 (1989) 179.
[10] E. Gorbova, V. Maragou, D. Medvedev, A. Demin, P. Tsiakaras, J. Power Sources 181 (2008) 207.
[11] M. Amsif, D. Marrero-López, J.C. Ruiz-Morales, P. Núñez, J. Power Sources 196 (2011) 3461.
[12] G. Ma, T. Shimura, H. Iwahara, Solid State Ionics 120 (1998) 51.
[13] A.N. Virkar, H.S. Maiti, J. Power Sources 14 (1985) 295.
[14] K.H. Ryu, S.M. Haile, Solid State Ionics 125 (1999) 355.
[15] W. Suksamai, I.S. Metcalfe, Solid State Ionics 178 (2007) 627.
[16] D.W. Lee, J.H. Won, K.B. Shim, Mater. Lett. 57 (2003) 3346.
[17] V. Agarwal, M. Liu, J. Mater. Sci. 32 (1997) 619.
[18] A.P. Almeida de Oliveira, J. Hafsaoui, J.-F. Hochepied, M.-H. Berger, A. Thorel, J. Eur. Ceram. Soc. 27 (2007) 3597.
[19] M. Amsif, D. Marrero-López, A. Magrasó, J. Peña-Martínez, J.C. Ruiz-Morales, P. Núñez, J. Eur. Ceram. Soc. 29 (2009) 131.
[20] C. Kleinlogel, L.J. Gauckler, Solid State Ionics 135 (2000) 567.
[21] D. Pérez-Coll, D. Marrero-López, P. Núñez, S. Piñol, J.R. Frade, Electrochim. Acta 51 (2006) 6463.
[22] X.-T. Su, Q.-Z. Yan, X.-H. Ma, W.-F. Zhang, C.-C. Ge, Solid State Ionics 177 (2006) 1041.
[23] Q.L. Ma, J.F. Gao, D.Y. Zhou, Y.J. Lin, R.Q. Yan, G.Y. Meng, Adv. Appl. Ceram. 107 (2008) 14.
[24] E. Gorbova, V. Maragou, D. Medvedev, A. Demin, P. Tsiakaras, J. Power Sources 181 (2008) 292.
[25] P. Babilo, S.M. Haile, J. Am. Ceram. Soc. 9 (2005) 2362.
[26] S. Tao, J.T.S. Irvine, Adv. Mater. 18 (2006) 1581.
[27] C. Peng, J. Melnik, J.-L. Luo, A.R. Sanger, K.T. Chuang, Solid State Ionics 181 (2010) 1372.
[28] E. Gorbova, V. Maragou, D. Medvedev, A. Demin, P. Tsiakaras, Solid State Ionics 179 (2008) 887.
[29] S. Ricote, N. Bonanos, Solid State Ionics 181 (2010) 694.
[30] R. Costa, N. Grünbaum, M.-H. Berger, L. Dessemond, A. Thorel, Solid State Ionics 180 (2009) 891.
[31] X'Pert HighScore Plus, version 2.2d, PANalytical BV 2004.
[32] J.C.C. Abrantes, Estereologia, Software Package ESTG/IPVC, Portugal, 2001.
[33] D. Johnson, "ZView: a Software Program for IES Analysis", Version 2.8, Scribner Associates, Inc., Southern Pines, NC, 2002.
[34] D. Marrero-López, J. Canales-Vázquez, J.C. Ruiz-Morales, A. Rodríguez, J.T.S. Irvine, P. Núñez, Solid State Ionics 176 (2005) 1807.
[35] J.E. Bauerle, J. Phys. Chem. Solids 30 (1969) 2657.
[36] T. Va Dijk, A.J. Burggraaf, Phys. Status Solidi A 63 (1981) 229.
[37] J.C.C. Abrantes, J.A. Labrincha, J.R. Frade, J. Eur. Ceram. Soc. 20 (2000) 1603.
[38] Y. Yamazaki, R. Hernandez-Sanchez, S.M. Haile, Chem. Mater. 21 (2009) 2755.
[39] D. Medvedev, V. Maragou, T. Zhuravleva, A. Demin, E. Gorbova, P. Tsiakaras, Solid State Ionics, doi:10.1016/j.ssi.2010.11.008.
[40] D. Pérez-Coll, P. Núñez, D. Marrero-López, J.C.C. Abrantes, J.R. Frade, J. Solid State Electrochem. 8 (2004) 644.